

A two-component ionized reflection model of MCG–6-30-15

D. R. Ballantyne,^{1,2*} S. Vaughan² and A. C. Fabian²

¹Canadian Institute for Theoretical Astrophysics, 60 St George Street, Toronto, Ontario, Canada M5S 3H8

²Institute of Astronomy, Madingley Road, Cambridge CB3 0HA

Accepted 2003 February 13. Received 2003 January 25; in original form 2002 November 28

ABSTRACT

Ionized reflection has often been considered as the explanation for the unusual Fe $K\alpha$ variability observed in MCG–6-30-15. In this paper, we test this model using a 325-ks observation of MCG–6-30-15 by *XMM–Newton* and *BeppoSAX*. The data are fitted between 2.5 and 80 keV with the constant-density models of Ross & Fabian. The best-fitting ionized reflection model requires the Fe $K\alpha$ line to be split into two reprocessing events: one from the inner disc to build up the red wing, and the other from the outer accretion disc to fit the blue horn. The implied geometry is a disc that becomes strongly warped or flared at large radii. A good fit was obtained with a solar abundance of iron and a reflection fraction (R) of unity for the inner reflector. The combination of the two reflection spectra can appear to have $R > 2$ as required by the *BeppoSAX* data. The inner reflector has an ionization parameter of $\log \xi = 3.8$, but the outer one is neutral with an inner radius of ~ 70 gravitational radii (r_g), corresponding to a light crossing time of approximately an hour for a $10^7 M_\odot$ black hole. Applying this model to time-resolved spectra shows that the inner reflector becomes more ionized as the source brightens. This reduces the strength of the red wing at high flux states. The X-ray source is constrained to arise from a narrow annulus at $\sim 5r_g$, with only 6 per cent of the 2–10 keV flux being due to the outer reprocessor. This amount of localized energy generation is extremely difficult to produce without resorting to other energy sources such as the black hole spin. In fact, all the Fe $K\alpha$ models fitted to *XMM–Newton* spectra of MCG–6-30-15 require a large increase in energy production at the inner edge of the accretion disc.

Key words: galaxies: active – galaxies: individual: MCG–6-30-15 – galaxies: Seyfert – X-rays: galaxies.

1 INTRODUCTION

X-ray observations of active galactic nuclei (AGN) allow for an unparalleled probe of the physics at the inner edge of the accretion disc. Spectral features such as a strong Fe $K\alpha$ line at 6.4 keV (see Reynolds & Nowak 2003 for a recent review) and a flattening of the power-law slope above ~ 10 keV (Pounds et al. 1990; Nandra & Pounds 1994) are indications that some fraction of the X-ray radiation is being reprocessed (or reflected) in optically thick material (e.g. George & Fabian 1991; Matt, Perola & Piro 1991). Using the *ASCA* observatory Tanaka et al. (1995) discovered a broad, asymmetric Fe $K\alpha$ line in the bright Seyfert 1 galaxy MCG–6-30-15 ($\tau = 0.008$) that was consistent with the profile expected from an emission line produced near 6 gravitational radii ($6r_g$; $r_g = GM/c^2$) from the black hole (Fabian et al. 1989; Laor 1991). Therefore, the reflection signatures observed in X-ray spectra of AGN are likely to be caused by reprocessing within the accretion disc – a plau-

sible scenario if the X-ray source resides in a hot corona above the disc (Galeev, Rosner & Vaiana 1979; Haardt & Maraschi 1991, 1993).

In the disc–corona geometry it is expected that the Fe $K\alpha$ line will respond rapidly ($\sim 50r_g$ s for a $10^7 M_\odot$ black hole) to any change in the continuum (Stella 1990; Matt & Perola 1992). Thus, the expectation is to observe a correlation between the line flux and the continuum flux, and a constant Fe $K\alpha$ equivalent width (EW). However, many long observations of MCG–6-30-15 have shown that the Fe line exhibits little variability (Lee et al. 2000; Reynolds 2000; Shih, Iwasawa & Fabian 2002; Fabian et al. 2002b) despite large (factors of 2–3) changes in the continuum flux, and an EW that decreases as the source brightens. Moreover, when variations were detected they were found to be uncorrelated with the continuum variability (Iwasawa et al. 1996, 1999; Vaughan & Edelson 2001). This perceived lack of Fe $K\alpha$ reverberation is a major challenge to the disc–corona model of X-ray production in AGN.

A possible solution to this problem is if the Fe line arises from the surface of a strongly photoionized accretion disc (Iwasawa et al. 1996; Lee et al. 2000; Reynolds 2000; Ballantyne & Ross 2002).

*E-mail: ballantyne@cita.utoronto.ca

When iron is highly ionized then increasing the strength of the illumination will result in a weaker Fe $K\alpha$ line relative to the continuum (see fig. 2 in Matt, Fabian & Ross 1996). The flux of the line can thus remain approximately constant despite variations in the driving continuum. This situation can occur when helium-like Fe is the dominant ionization state (Matt, Fabian & Ross 1993; Ballantyne, Fabian & Ross 2002), and thus requires the disc surface to have a high ionization parameter, $\log \xi > 3$, where $\xi = 4\pi F_X/n_H$. The major difficulty with this solution is that the He-like Fe $K\alpha$ line occurs at 6.7 keV, but the line core of MCG–6-30-15 is well established to be at 6.4 keV, and does not arise from very distant material (Lee et al. 2002). Therefore, at first glance it seems unlikely that the Fe $K\alpha$ line arises from an ionized disc.

One way to check this interpretation is to compare the entire spectrum with models of X-ray reflection from accretion discs. Calculations of X-ray reprocessing have shown that the shape of the spectrum is sensitive to the ionization state of the material (Ross & Fabian 1993; Ross, Fabian & Young 1999), its density distribution (Nayakshin, Kazanas & Kallman 2000; Ballantyne, Ross & Fabian 2001b; Dumont et al. 2002; Rózańska et al. 2002), and the properties of the illuminating radiation (Ballantyne & Ross 2002). These models self-consistently calculate the strength of the Fe $K\alpha$ line, which changes as a function of ionization state and abundance (Ballantyne et al. 2002), so the line and the entire continuum can be fitted simultaneously with only a few parameters.

This exercise was previously performed for MCG–6-30-15 by Ballantyne & Fabian (2001) using *ASCA* data. They found that the data between 3 and 10 keV (the 3-keV cut-off was used to avoid the warm absorber) was well fitted by an ionized reflector, but required the addition of a separate line component further out along the disc. However, a good fit was also obtained by a single, neutral constant-density reflector with twice the solar iron abundance. From those data it was unclear which interpretation was more plausible.

Producing a physical model for the X-ray spectrum and spectral variability of MCG–6-30-15 is highly involved and there is no unique solution to this problem. In this paper we explore the implications for models in which the spectrum is dominated by features from a photoionized accretion disc. Specifically, we improve on the results of Ballantyne & Fabian (2001) and develop a model for the spectrum of MCG–6-30-15 in terms of reflection from two distinct sites on the disc and test this model against the observed spectral variability. An alternative model, in which the reflection spectrum is physically disconnected from the continuum due to relativistic effects, is discussed by Fabian & Vaughan (2002). We make use of data obtained from a 325-ks observation of MCG–6-30-15 by *XMM-Newton* and from a simultaneous observation by *BeppoSAX* (Fabian et al. 2002b).

In the next section, the data and models are briefly introduced. In Section 3 we use the broad-band *BeppoSAX* data to constrain the reflection spectrum in a manner independent of the iron line. Section 4 presents the results of the ionized disc fits. The findings are discussed in Section 5 before conclusions are presented in Section 6.

2 DATA AND MODELS

Details of the observations are given in Fabian et al. (2002b). For the present paper the data were processed using *XMM-Newton* Science Analysis System (SAS) v5.3.3, with source data extracted from circular regions of radius 35 arcsec from the EPIC MOS and pn. Background events were extracted from off-source regions. Events corresponding to patterns 0–12 (single–quadruple pixel events) were extracted from MOS and patterns 0–4 (singles and doubles) were

used for the pn analysis, after checking for consistency with the data extracted using only single-pixel events (pattern 0). Standard redistribution matrices (m1_r6.all_15.rmf) for MOS1 (similarly for MOS2) and (epn_sw20_sdY9.rmf) for the pn were used, and ancillary response files were generated using ARFGEN v1.48.8.

The additional calibration information included in this version of the SAS now allow the use of the pn data (in Fabian et al. 2002b only the MOS data were analysed). However, it was found there was a small but significant difference in photon index ($\Delta\Gamma \sim 0.1$) between the MOS and pn spectra even after removing the small amount of pile-up in the MOS data. Since the value of Γ obtained from the pn data was more consistent with that from the MECS and PDS instruments, we ignored the MOS data in this analysis (see Fabian & Vaughan 2002, for further discussion of the EPIC data).

The constant-density ionized reflection models of Ross & Fabian (1993) and Ross et al. (1999) were used in the spectral fitting, as these are the most useful in parametrizing the shape of the spectrum. Models where the accretion disc atmosphere is in hydrostatic balance (e.g. Nayakshin et al. 2000; Ballantyne et al. 2001b; Rózańska et al. 2002) were not used because they are dependent on the unknown accretion disc structure. However, Ballantyne et al. (2001b) found that the hydrostatic models could be fitted with dilute versions of the constant-density ones. Therefore, there is no significant difference in the shape of the reflection spectrum between the two cases.

XSPEC v11.2 (Arnaud 1996) was used for all spectral fitting, and we use the 90 per cent confidence level to compute error bars for the fitting parameters.

3 THE REFLECTION STRENGTH

As a first step toward determining the properties of the reflection spectrum in MCG–6-30-15, the high-energy *BeppoSAX* PDS data were examined in order to constrain the strength of the Compton reflection ‘hump’. In this analysis models of the reflected continuum were compared with the PDS data over the 14–200 keV range, which includes the peak of the reflection spectrum. The MECS data were included in the fitting to better constrain the slope of the underlying continuum. Only MECS data in the ranges 2.5–3.5 and 7.5–10.0 keV were used as these should be dominated by the primary X-ray continuum; the spectrum is complicated by absorption below 2.5 keV and the strong, broad iron line in the ~ 3 –7 keV range. The normalization of the PDS data was tied to 0.86 times the MECS value (Fiore, Guainazzi & Grandi 1999). The EPIC data were not included in these fits as the much higher signal-to-noise ratio of these data would mean the model parameters would be determined almost entirely by the low-energy EPIC data, not the PDS.

A simple power-law model for the broad-band continuum provided a poor fit to the data ($\chi^2 = 170.7/46$ degrees of freedom, d.o.f.), with a photon index of $\Gamma = 1.85$. The residuals from this fit showed that the PDS data were systematically in excess of this model in the 14–40 keV range, a strong indication of the presence of an additional Compton reflection continuum, which peaks at ~ 30 keV. Allowing for an exponential cut-off in the power-law continuum did not improve the fit ($\chi^2 = 170.7/45$ d.o.f.) and gave a best-fitting cut-off energy $E_{\text{cut}} > 500$ keV, i.e. above the band-pass of the data, implying that the high-energy spectral curvature is not the result of a roll-over in the power-law continuum. This fit is illustrated in Fig. 1. The earlier *BeppoSAX* observation reported by Guainazzi et al. (1999) also clearly detected the reflection continuum of MCG–6-30-15.

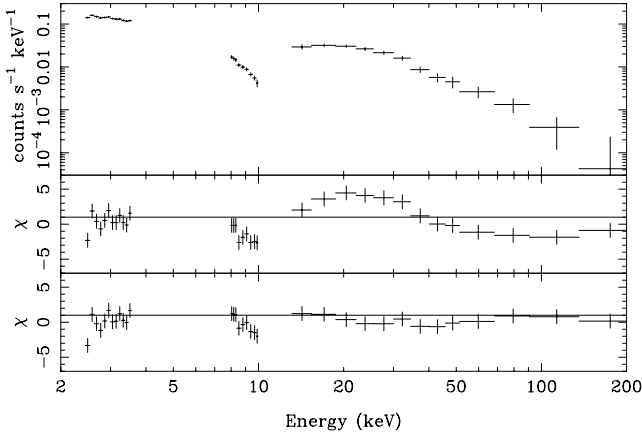


Figure 1. Top panel: *BeppoSAX* PDS and MECS data. Middle panel: residuals from a fit using an exponentially cut-off power-law model. Bottom panel: residuals allowing for reflection as described in Section 3.

The broad-band spectrum was therefore modelled in terms of a power-law plus Compton reflection continuum. The PEXRAV model (Magdziarz & Zdziarski 1995) was used to compute the spectrum. Specifically, this computes the spectrum resulting from an exponentially cut-off power-law continuum incident on a slab of optically thick, neutral material, accounting for Compton reflection and bound-free absorption. Unlike the Ross & Fabian (1993) ionized disc model, PEXRAV does not account for discrete emission features (specifically, fluorescence and recombination emission). However, it does account for the angular dependence of the reflected spectrum and the reflection of incident photons with energies $\gtrsim 100$ keV (which requires relativistic corrections to the scattering cross-section; White, Lightman & Zdziarski 1988). This model should therefore be appropriate for the energy ranges included in the fitting, which extend above 100 keV and ignore regions containing strong atomic emission features.

Including a PEXRAV reflection component in the model improved the fit substantially ($\chi^2 = 71.7/44$ d.o.f.) and gave the following fit parameters: $\Gamma = 2.17 \pm 0.10$, $E_{\text{cut}} > 143$ keV and a normalization of the reflected spectrum relative to the primary continuum of $R = 2.7^{+1.4}_{-0.9}$, where $R = \Omega/2\pi$. The inclination angle of the reflector was fixed at $i = 30^\circ$ (Tanaka et al. 1995; Fabian et al. 2002b) and the abundances were assumed to be solar. This fit suggests rather strong reflection; an isotropic continuum source illuminating a flat accretion disc would be expected to yield a relative reflection strength of $R \sim 1$ (i.e. the reflector subtends a solid angle $\Omega \sim 2\pi$ as seen by the continuum source).

The exact strength and shape of the observed reflection spectrum does, however, also depend on the abundances of the reflector, its inclination and its ionization state. The effects of these parameters on the measured value of R were investigated as follows. The PEXRAV model was re-fitted to the data with the Fe abundance fixed at $3\times$ and then $7\times$ solar and also with the Fe abundance as a free parameter. The $3\times$ solar model made the largest improvement to the fit (compared with the solar case) and the best-fitting abundance value was $3.5^{+1.4}_{-1.9}$. This gave $\chi^2 = 63.6/44$ d.o.f. and the reflection fraction was constrained to be $R > 2.6$ (this fit is shown in the bottom panel of Fig. 1). Allowing the abundances of elements lighter than Fe to vary did not improve the fit further. The Fe abundance was therefore fixed to be $3\times$ solar in the remaining PEXRAV models. Lee et al. (1999) previously presented evidence for an enhanced iron abundance in MCG–6-30-15.

The apparent strength of the reflected spectrum, for a given value of R , is also dependent upon the inclination angle of the reflector with respect to the line of sight (e.g. fig. 5 of Magdziarz & Zdziarski 1995). Allowing the inclination angle to be a free parameter gave only a small improvement in the quality of the fit ($\chi^2 = 63.4/43$ d.o.f.) with $i < 80^\circ$ and similar constraints on the reflection strength $R > 2.8$.

The final possibility explored to explain the high value of R was ionization of the reflector. This was performed by using the PEXRIV model and allowing the ionization parameter ξ to vary (with $3\times$ solar Fe and $i = 30^\circ$). This gave only a slight improvement in the fit ($\chi^2 = 61.8/43$ d.o.f.) with $\xi < 200$ and $R > 2.8$ [this ξ has been corrected for the different energy ranges used in PEXRIV and the model of Ross & Fabian (1993)]. The low value of ξ means that the lack of Comptonization of the Fe K edge in this model will not affect the limit on R . Thus, even allowing for the possible effects of non-solar abundances, angular dependence and ionization on the reflection spectrum, the strength of the reflection measured using the high-energy PDS data appeared to be $R \gtrsim 2$. This constraint on R is independent of the possible presence of a roll-over in the power-law continuum, since the cut-off energy of the power law was a free parameter in the above fits.

4 IONIZED REFLECTION RESULTS

The *BeppoSAX* constraint on R is difficult to explain in terms of the standard disc-corona geometry, which predicts $R \sim 1$. A large reflection strength can be generated if the X-ray-emitting plasma is moving towards the accretion disc at mildly relativistic velocities (Reynolds & Fabian 1997; Beloborodov 1999; Malzac, Beloborodov & Poutanen 2001). However, this model would predict an extremely soft $\Gamma > 2.2$ spectrum for MCG–6-30-15, which is not observed. Another method of obtaining a large value of R was given by Fabian et al. (2002a) who considered the results of reflection from a lumpy or corrugated accretion disc (see also Ross, Fabian & Ballantyne 2002). In this scenario, the optically thick disc may subtend a solid angle larger than 2π as seen from the X-ray source. Again, softer spectra are naturally predicted from such geometry, as the hard X-ray source ‘sees’ more ultraviolet (UV) photons from the disc.

When fitting the *ASCA* spectra of MCG–6-30-15, Ballantyne & Fabian (2001) found that it was very difficult for an ionized Fe $K\alpha$ line to fully account for both the strength and width of the observed feature. On the other hand, an ionized reflection continuum provided a good fit to the observed one, including the red wing of the Fe $K\alpha$ line. Thus, Ballantyne & Fabian (2001) were forced to consider a two-component model, where the red wing was fitted by the ionized reflector, and the line core by a neutral disc line at 6.4 keV. Misra (2001) has also considered a two-component model of the MCG–6-30-15 iron line. A superposition of more than one reflection event may also account for the observed reflection strength. In this section, we investigate the validity of such a model with our high signal-to-noise ratio *XMM-Newton* data.

4.1 The time-averaged spectrum

MCG–6-30-15 has a strong warm absorber that significantly affects the continuum below 2–3 keV (Nandra & Pounds 1992; Reynolds et al. 1995; Lee et al. 2001; Sako et al. 2002). Therefore, the use of the full pn spectrum would necessitate a complete model of the warm absorber from analysis of the reflection grating spectrometer (RGS) data. However, the strongest reflection features are not

affected by the warm absorber, so, following Ballantyne & Fabian (2001) and Fabian et al. (2002b), we only considered data above 2.5 keV. The MECS and pn data were cut-off at 10 and 12 keV, respectively. The PDS data were cut-off at 80 keV because the Ross & Fabian (1993) models have a high-energy limit of 100 keV. All fits included the Galactic absorbing column of $4.06 \times 10^{20} \text{ cm}^{-2}$ (Elvis, Wilkes & Lockman 1989). Data from the three instruments were fitted simultaneously with the normalizations free except for the PDS which was fixed to be 0.86 times the MECS value as in Section 3.

The model consisted of the sum of two reflection spectra with solar iron abundance. The first of these components was relativistically blurred with a Laor (1991) kernel that had a power-law emissivity ($\propto r^{-\beta}$) with the index frozen at $\beta = 3$. The second component was also blurred, but with a flatter index of $\beta = 2$ appropriate for the case when the disc is warped and emission from large radii is non-negligible. Both reflectors were illuminated by the same power-law spectrum, but this primary emission was included only in the first component where it was added in so that R was unity. Thus, the second component was reflection dominated. In this way, a total observed $R > 2$ can be obtained, as required by the *BeppoSAX* data (Section 3). Following Fabian et al. (2002b) a Gaussian with zero width was included at 6.9 keV to fit an additional spectral feature.

The best fit obtained with this model is shown in Fig. 2 and Table 1. We find a very good fit to the data ($\chi^2/\text{d.o.f.} = 1600/1879$)

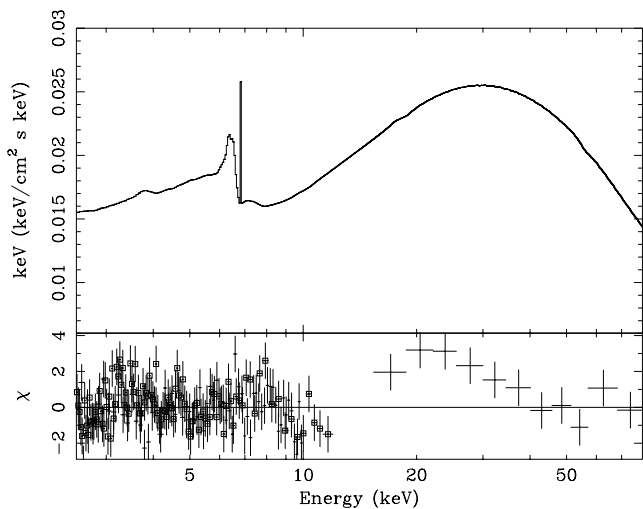


Figure 2. The summed double-reflector model fit to MCG-6-30-15 between 2.5 and 80 keV. The top panel shows the total spectrum in $E_F E$ space (see Fig. 5 for a plot showing the model components), and the lower panel are the residuals in units of standard deviations. The pn data are shown with the open symbols, and the fit parameters are displayed in Table 1. The residuals at 20–30 keV are a result of the reflection spectra being angle-averaged, which reduces the strength of the reflection hump (Magdziarz & Zdziarski 1995) for inclination angles $< 50^\circ$.

Table 1. The parameters for the best-fitting time-averaged double-reflection model shown in Fig. 2. Γ is the photon index of the incident power-law continuum, ξ is the ionization parameter of the reflector, r_{in} is the inner radius of the reflector in r_g , r_{out} is the outer radius (also in r_g), and i is the inclination angle in degrees. The EWs of the 6.4-keV line and the narrow 6.9-keV line are given in eV. The EW of the broad Fe $K\alpha$ line includes both components to the line profile. The inner reflector had R fixed at unity, and an emissivity of $\beta = 3$. The outer component was reflection dominated and had an emissivity of $\beta = 2$. p means the parameter pegged at its lower limit.

Γ	Inner reflector			Outer reflector			i	EW _{6.4 keV}	EW _{6.9 keV}	$\chi^2/\text{d.o.f.}$
	$\log \xi$	r_{in}	r_{out}	$\log \xi$	r_{in}	r_{out}				
$1.92^{+0.02}_{-0.01}$	$3.82^{+0.02}_{-0.03}$	4.93 ± 0.01	$5.012^{+0.003}_{-0.002p}$	< 1.07	71^{+64}_{-33}	1822^{+1425}_{-732}	$31.6^{+0.8}_{-1.0}$	450	29^{+31}_{-5}	1600/1879

with an ionized reflector located at approximately $5r_g$ and a neutral reflector outside of $\sim 70r_g$. The photon index is consistent with the results of Fabian et al. (2002b) ($\Gamma = 1.95$; see their table 1). The inner radius found here ($\sim 5r_g$) is further out than that found by Wilms et al. (2001) or Fabian et al. (2002b) ($\sim 2r_g$). This is because the ionized reflection model has both a curved spectrum and an intrinsically broadened Fe $K\alpha$ line (due to Comptonization). The ionization parameter of the inner reflector ($\log \xi = 3.82$) is such that He-like iron is the dominant ion at the surface of the disc. Therefore, the rest energy of the Fe $K\alpha$ line is at 6.7 keV, but is gravitationally redshifted down to below 6 keV.

Examining the residuals to this fit in Fig. 2 shows that the reflection hump is not accurately reproduced. This problem is due to the fact that the Ross et al. (1999) reflection models are angle-averaged rather than computed for a specific inclination angle (as is done in PEXRAV). For angles $< 50^\circ$, angle-averaging results in a weaker reflection hump at 20–30 keV (Magdziarz & Zdziarski 1995). A possible secondary effect is the hard 100 keV cut-off in the Ross et al. (1999) models, causing the spectrum to turn downwards faster than is observed. However, cutting off the PDS data at lower energies (say, 40–50 keV) has little impact on the model parameters. Despite these issues, Fig. 2 illustrates that more than one reprocessing event can account for the strong reflection hump observed in the *BeppoSAX* data.

Allowing β for the inner reflector to be a free parameter does not improve the fit for any value between 10 and -10 because the inner and outer radii are so close together (see below). Doing the same for the outer component improves the fit only slightly with $0.641 \leq \beta_{\text{out}} \leq 2.268$. This result emphasizes that the model requires a flat emissivity at large radii, consistent with a strongly warped or concave disc. Allowing the reflection fraction to be free does drop the χ^2 by 8, which is significant at 99.8 per cent according to the F -test. The best-fitting value of R in this case is $1.98^{+0.97}_{-0.44}$. This additional reflection only affected the fit around the Fe $K\alpha$ line, and did not alter the residuals at higher energies.

In this model, the large red wing of the Fe line and the 2–10 keV continuum are due to the inner ionized reflector, while the blue core of the line and the reflection hump are dominated by the outer reprocessor. The most striking feature of this fit is that the radii over which the inner component originates is restricted to a narrow annulus only $0.08r_g$ wide. In Section 5.2 we discuss the implications of this model and attempt to evaluate whether it is physically plausible.

4.2 Time-resolved spectra

In order to investigate whether the double-reflector model can explain the spectral variability properties of MCG-6-30-15, we split the *XMM-Newton* data set into 32 10-ks segments (see Fig. 3). Source and background spectra were extracted from the pn for each interval. As a result of the ~ 71 per cent observing efficiency of

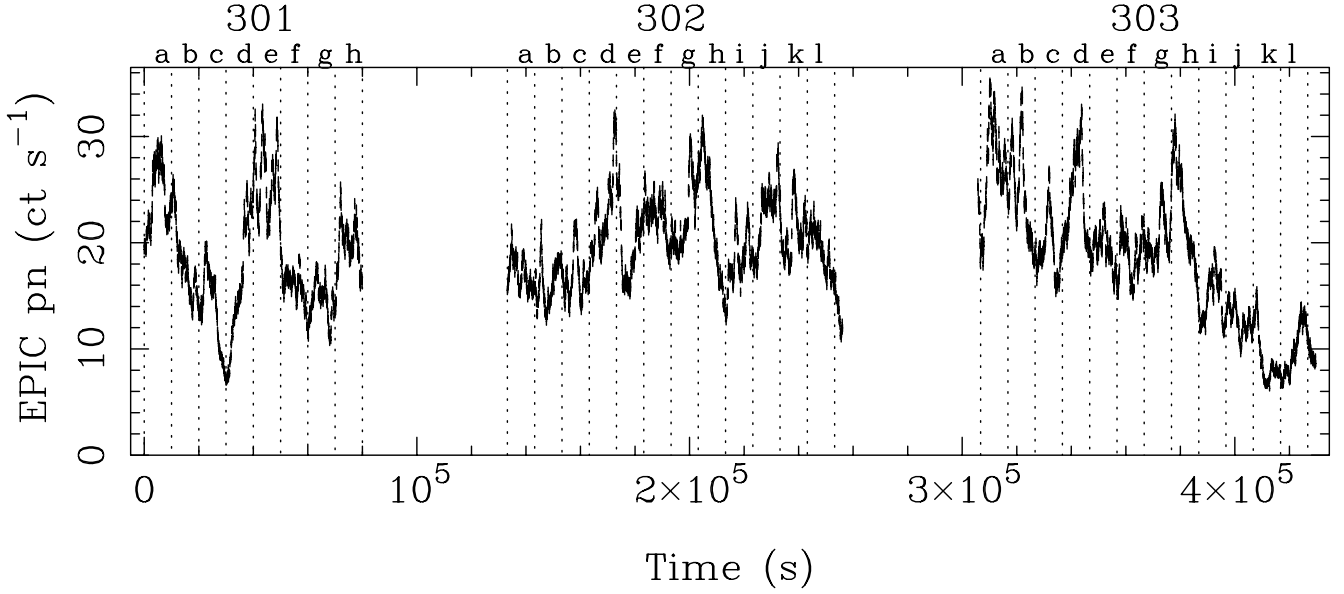


Figure 3. *XMM-Newton* EPIC pn light curve (0.2–10 keV) of MCG-6-30-15. The dotted lines denote the 10-ks segments discussed in the text. Source and background spectra were extracted from each segment. The total good exposure time of each spectrum was ~ 7.1 ks due to the live-time of the pn in small window mode. The count rates in this figure have not been corrected for this scalefactor.

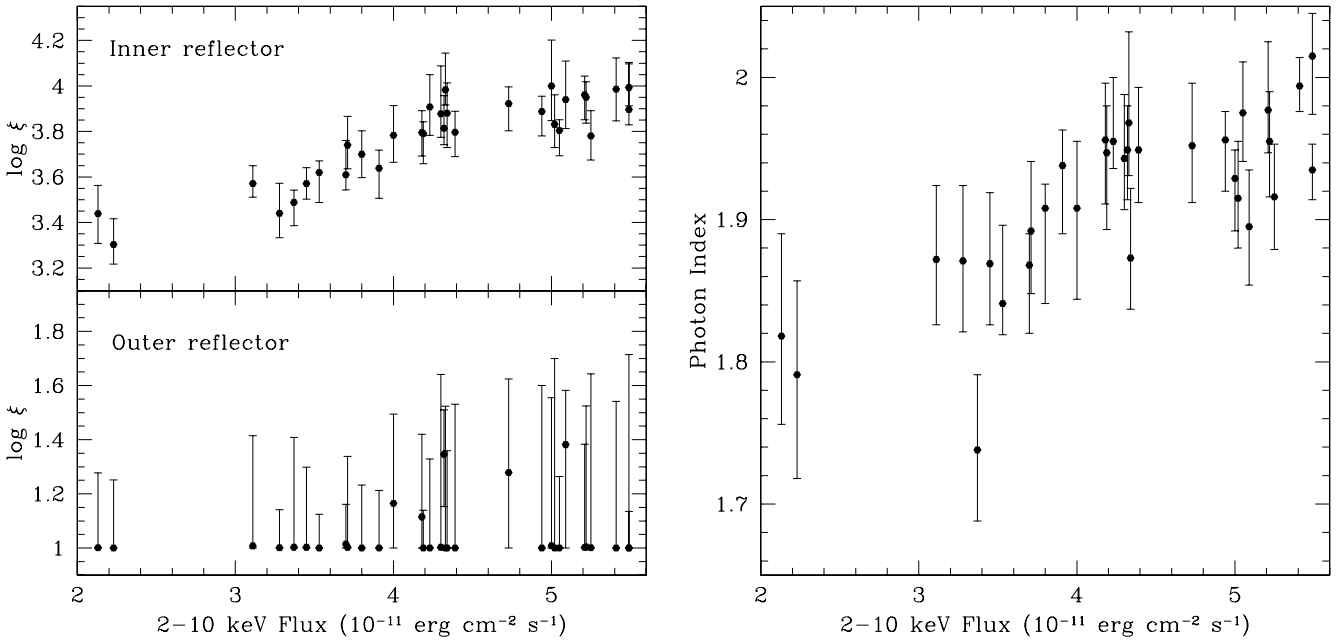


Figure 4. Left: plot of the ionization parameter for the two reflectors versus the total 2–10 keV flux. The inner reprocessor clearly become more ionized as the source becomes brighter, while the distant reflector remains neutral. Right: plot of the photon index (Γ) versus the total 2–10 keV flux. The source becomes softer as it brightens, which is in agreement with many other observations of MCG-6-30-15 using simpler models.

the pn (Strüder et al. 2001), the exposure time of each spectrum was ~ 7.1 ks.

Each of the 32 spectra were fitted with the double-reflection model between 2.5 and 12 keV using the time-averaged results (Table 1) as a template. All parameters were allowed to float, except for the inner and outer radii of the distant reflector, the reflection fraction R and the inclination angle i , which were all fixed at the values listed in Table 1. Keeping R fixed allows us to test whether the data are consistent with the innermost reflection component varying (in flux) along with the

continuum (allowing for changes in the ionization parameter). The emissivity indices also remained unchanged from the time-averaged fitting. The model provided an acceptable fit (reduced $\chi^2 \sim 1$) to the continuum and Fe $K\alpha$ line for each spectrum.

The results from this fitting are shown in Fig. 4. The left-hand panel shows the ionization parameter of the two reflectors as a function of the total 2–10 keV flux calculated from the model. This plot clearly shows that the inner reprocessor at $\sim 5r_g$ becomes more ionized as MCG-6-30-15 becomes brighter. The relationship between

ξ and the flux is roughly linear over most of the plot. The red wing of the Fe $K\alpha$ line (which is fitted by this reflector) will therefore be weak at high flux levels. In contrast, the ionization parameter of the outer reflector is uncorrelated with the 2–10 keV flux and remains small, consistent with predominantly neutral reflection. The right-hand panel in Fig. 4 plots Γ as a function of 2–10 keV flux. Here, we see that we have recovered the well-known property that the spectrum of MCG–6–30–15 softens as it becomes brighter (e.g. Vaughan & Edelson 2001; Shih et al. 2002).

5 DISCUSSION

XMM–Newton has observed MCG–6–30–15 twice. The first observation showed the broad iron line probably extends down below 4 keV, implying emission from within $6r_g$, and also showed a narrower core to the line (Wilms et al. 2001). This apparent two-component line may suggest that there is reflection from two distinct sites. The second reprocessing site is unlikely to be very distant (e.g. the molecular torus postulated in Seyfert unification schemes) as the high-resolution *Chandra* HETGS spectrum showed little flux from an intrinsically narrow line component (Lee et al. 2002). The second, longer *XMM–Newton* observation also appeared to show line emission extending down to low energies. Fabian et al. (2002b) modelled this in terms of neutral reflection from an accretion disc with a broken power-law emissivity profile. In this model the extended red wing of the line is produced by emission within $6r_g$, while the core of the line profile (which was resolved) is produced from reflection beyond $6r_g$ and with a relatively flat emissivity profile. These analyses both suggest that the core of the line around 6.4 keV is mostly produced by reflection off material at distances of ~ 6 – $1000r_g$, while the red wing of the line is produced by emission from within $6r_g$. Such an interpretation is consistent with the ionized reflection results found above. In this section we consider the two-component ionized disc model in detail.

5.1 General comments

In Section 4 it was found that ionized reflection models can fit the *XMM–Newton* data of MCG–6–30–15 but only with some difficulty. As was found previously (Ballantyne & Fabian 2001), it is difficult for the predicted spectrum to account for the strength and width of the Fe $K\alpha$ line, and the smooth continuum. The most tenable model required a secondary reflector from further out on the disc, but, more worryingly, the region of primary X-ray generation is confined to a very narrow annulus. Are there limitations in our reflection spectra which are resulting in these extreme models? Although it is difficult to answer this question definitively because the detailed physics of AGN is relatively unknown, the Ross & Fabian (1993) reflection models have been very successful in fitting the X-ray spectra of many different Seyferts (Ballantyne, Iwasawa & Fabian 2001a; Orr et al. 2001; De Rosa, Fabian & Piro 2002a; De Rosa et al. 2002b). On the computational side, the code has been compared with similar angle-averaged reflection calculations (Péquignot et al. 2001) and there was good agreement at hard X-rays, particularly around the Fe $K\alpha$ line. The models used here assume reflection from a constant-density slab, rather than a variable density atmosphere, as was done in Ballantyne & Fabian (2001). In these variable density models weaker Fe $K\alpha$ lines are expected due to the smaller density at the surface of the disc; therefore, a constant-density slab, although perhaps unrealistic, is the ‘best case scenario’ for producing strong Fe $K\alpha$ lines. Thus, it seems unlikely that this extreme fit is a result of limitations in the reflection models.

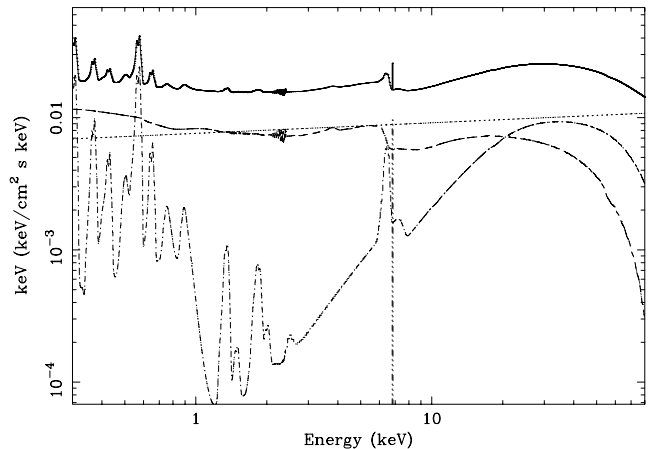


Figure 5. The time-averaged reflection spectrum between 0.3 and 80 keV predicted by the double-reprocessor model discussed in Section 4.1. Galactic absorption has been removed in order to show the soft X-ray lines predicted by the model. The solid line is the full model; the dashed line denotes the inner, ionized reflector; the incident $\Gamma = 1.92$ power law is shown with the dotted line, and the outer, neutral reprocessor is the dot-dashed line. The 6.9 keV result is also included in the plot. The noise at ~ 2 keV is a plotting artefact that did not affect the spectral fit.

It is worth pointing out that, consistent with the results of Wilms et al. (2001) and Fabian et al. (2002b), the Fe $K\alpha$ line profile in this model suggests a concentration of emission from within $\sim 5r_g$. It is unknown whether this is from the plunge region of a Schwarzschild black hole, or from the disc around a spinning Kerr hole. In either case, it seems as though additional physics must be included into our thinking of energy generation in AGN.

5.2 Implications of a double-reflection model

5.2.1 Observational testable predictions

In Fig. 5 the double-reflection model is broken into its components and plotted between 0.3 and 80 keV. Absorption from the Galaxy has been removed so that the soft X-ray spectral features can be seen unhindered. The total 2–10 keV flux given by the model is 4.36×10^{-11} erg cm $^{-2}$ s $^{-1}$, of which only 6 per cent is contributed by the distant component. When the energy range is extended to 100 keV, the outer reflector provides 21 per cent of the total flux. Thus, if this model is viable we would expect a decrease in rapid continuum variability at higher energies, as the more distant emission would contribute to a larger fraction of the total spectrum. Furthermore, there may be a detectable lag in variations at high energies compared with those occurring between 2 and 10 keV. These predictions could be tested by *Integral* or *ASTRO-E2*.

Another observationally testable aspect of this model are the soft X-ray spectral features. The ionization parameter of the outer reflector is constrained to be small enough for iron to be only weakly ionized, but in these cases recombination emission from ions of highly ionized metals such as C, N and O are common at lower energies (Ross & Fabian 1993). As there is only an upper limit on the ξ of the outer component, we cannot predict the exact lines that may be present in the total spectrum. However, as an example, the EWs of the soft X-ray lines relative to the total predicted continuum are shown in Table 2 for the case when $\log \xi = 1.0$. The strongest line is predicted to come from O VII with an EW of ~ 36 eV. Once an accurate model for the warm absorber has been

Table 2. Equivalent widths of the soft X-ray emission lines predicted by the double-reflection model when $\log \xi = 1.0$ for the outer reflector.

Line	EW (eV)
Si K α	6
Mg K α	4
O VIII Ly α	9
O VII	36
N VI	6
C VI Ly α	9

determined it should be possible to search for such a line in the current data set. The line is not extremely relativistically blurred, so may even stand out in the RGS spectra and would be unrelated to the relativistic soft X-ray line model of Branduardi-Raymont et al. (2001).

In Section 4.2 it was found that the ionization parameter of the inner reflector was correlated with the 2–10 keV flux and was always greater than 1000. This implies that the strength of the iron line (which comprises the red wing of the observed Fe K α line) is anticorrelated with the flux (Matt et al. 1996; Ballantyne et al. 2002). However, if the flux of MCG–6-30-15 drops to approximately one-half of the faintest level observed here so that $\log \xi < 3$, then the strength of the red wing correlates with ξ . This is another observational testable feature.

5.2.2 Geometry

The geometry implied by the double-reflector fit requires two different changes in curvature in the accretion disc. First, the disc must become strongly concave at a radius of $\sim 50\text{--}70r_g$ to provide the surface for the second reflection component. A standard Shakura–Sunyaev gas-pressure-dominated accretion disc is already mildly concave with the scaleheight $H \propto r^{9/8}$ (Shakura & Sunyaev 1973), but a warp much larger than this is required to substantially increase the reprocessed flux (see fig. 2 in Blackman 1999). A possible mechanism may be warping due to radiation pressure on the disc (Pringle 1996, 1997), however, the typical transition radius for this instability is $\sim 1000r_g$ for an AGN disc (Pringle 1997). The Bardeen–Peterson effect (Bardeen & Peterson 1975; Kumar & Pringle 1985), which aligns the inner part of an accretion disc so that it is perpendicular to the spin axis of the central object, is another possible method to warp a disc if the outer regions are not in the equatorial plane. The transition radius for this mechanism is $\lesssim 100r_g$ (Ivanov & Illarionov 1997; Nelson & Papaloizou 2000), so the Bardeen–Peterson effect can account for the outer disc geometry implied by the double-reflection model. Of course, a spinning black hole would be needed to cause this effect.

Another constraint on the geometry is provided by the inner reflector. Here, the emission is confined to a narrow ring at $\sim 5r_g$ (see Section 5.2.4) and there is no reprocessing between that point and the outer disc, 10 times further away. This implies that the inner X-ray source is hidden from most of the inner accretion disc, which requires the scaleheight to rise quickly at $\sim 5r_g$. A schematic diagram illustrating this geometry is shown in Fig. 6. The increase in disc thickness could be due to an increase in the radiation pressure support in the innermost region of the accretion flow.

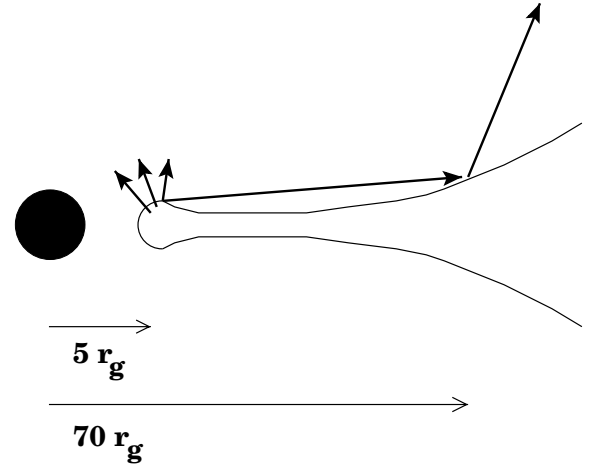


Figure 6. A schematic representation of a possible geometry implied by the double-reflection model. X-rays are produced at the inner edge of the accretion flow which is thicker than the rest of the inner disc (possibly because of large radiation pressure support). Reflected emission from this environment is greatly blurred and highly ionized. The increased height shields the inner disc from much of the direct radiation, and it is not until the disc becomes more concave at large radii that it produces more reflection.

5.2.3 Fe K α variability

The most intriguing aspect of the double-reflector model is its potential to possibly explain the puzzling variability of the Fe K α line profile (Iwasawa et al. 1996, 1999). Analysis of the long (4.5-d) 1994 *ASCA* observation of MCG–6-30-15 by Iwasawa et al. (1996) considered the variability of the line core separately from the broad red wing. They found that on time-scales greater than a few 10^4 s, the narrow component seemed to increase with the continuum flux, while the strength of the broad component decreased. On shorter time-scales of a few 10^3 s the broad component varied, but the narrow core was consistent with staying constant. Reinforcing these trends was the spectral evidence provided by examining the data during flares or dips in the light curve. Iwasawa et al. (1996) found that during a bright flare, the spectrum (integrated over 36 ks) showed a strong line core, but a very weak red wing. In contrast, a 15-ks deep minimum at the end of the observation showed a strong red wing and a weak blue core. Another interesting line profile was found during a bright, hour long flare in the 1997 long *ASCA* observation of MCG–6-30-15. Iwasawa et al. (1999) reported that the spectrum extracted from the flare had line emission only from within $5r_g$. There was little evidence for a core at 6.4 keV, with a limit on the EW of 60 eV.

A long 400-ks *RXTE* observation also illustrated the strange behaviour of the Fe K α line in MCG–6-30-15. Although the PCA on *RXTE* could not resolve the line into a core and wing, these data were used by Lee et al. (2000) and Reynolds (2000) to search for variations in the line flux with the continuum. Both studies found that much of the line flux was constant and unresponsive to large continuum changes down to time-scales as low as perhaps 0.5 ks. Vaughan & Edelson (2001) fitted these data on the orbital time-scale of *RXTE* and found variations in the line flux, but these were also uncorrelated with the continuum. Fabian et al. (2002b) found a similar result using this *XMM-Newton* observation. These authors subtracted a 10-ks low flux state spectrum from a 10-ks high flux state one and found that the difference was well fitted by a power law. The constancy of the Fe K α line flux, which has been seen in

other Seyfert 1s (e.g. NGC 5548; Chiang et al. 2000), is hard to understand if the entire line arises from close to the primary X-ray source.

Analysis of time-resolved *XMM-Newton* spectra using the double-reflection model found that the inner component became more ionized when MCG–6–30–15 was brighter (the left-hand panel of Fig. 4). Recall from Fig. 5 that the spectrum between 2.5 and 12 keV is dominated by emission from the inner zone. Also, the shape of an ionized reflection spectrum changes with ξ (Ross et al. 1999). Thus, the change in ionization parameter found in the inner reflector is due to variations in the shape of the spectrum, and not just the Fe $K\alpha$ line. This is not necessarily an obvious result. MCG–6–30–15 softens as it becomes brighter (see the right-hand panel of Fig. 4), and a steeper illuminating power law will decrease the ionization state of the reflector at a constant irradiating flux. Therefore, in order for ξ to increase the incident flux must grow at a rate fast enough to offset the changes in the spectral slope.

As the ionized reflector is nearly coincident with the X-ray source in this model, reverberation would be large on short time-scales, adjusting the shape of the line. Therefore, assuming a constant R , the changes in the Fe $K\alpha$ line profile observed by *ASCA* can be explained by changes in the ionization state of the inner reflector (see also Reynolds 2000). When the source is bright, the reprocessing zone becomes highly ionized and the amplitude of the red wing diminishes. On the other hand, when the source is in a low state, the ionization parameter drops and there is more emission from the red wing, explaining the results of Iwasawa et al. (1996). However, can the blue core from the distant, neutral reflector respond on the correct time-scale to explain its variations? The best-fitting inner radius for the outer reflector is $71r_g$ (Table 1). This corresponds to a light-crossing time of $3.5M_7$ ks, where $M_7 = M/10^7 M_\odot$. Iwasawa et al. (1999) saw no blue core in their 1997 *ASCA* flare spectrum, which lasted approximately an hour – the same time-scale estimated above. Therefore, increasing the black hole mass by only a small amount will comfortably explain this observation. Yet Fabian et al. (2002b) found that the difference between a high- and low-state spectrum of MCG–6–30–15 is consistent with a power law. The conclusion from that test is that the Fe $K\alpha$ line must not have changed strength or shape between the two states.

To investigate the line variability predicted by the ionized disc model more closely, we show in Fig. 7 three examples of a difference spectrum obtained by subtracting the best-fitting double-reflector model for a low flux state segment from the model of a high-state segment. Dips in these spectra correspond to regions where the feature was stronger in the low flux state than in the high flux state, and bumps correspond to areas where the high flux model was stronger than the low flux model. The difference spectra obtained from the data were unfolded and plotted in Fig. 7 to illustrate their statistical quality.

The bottom panel shows the difference between the models for Rev. 301:e and 301:f (see Fig. 3). At the end of 301:e there is sudden drop from a 2–10 keV flux of 5.21×10^{-11} erg cm $^{-2}$ s $^{-1}$ to 3.07×10^{-11} erg cm $^{-2}$ s $^{-1}$ in ~ 1000 s. The ionization parameter of the inner reflector fell from $\log \xi = 3.96$ to 3.61 over that interval, as did the photon index: $\Gamma = 1.98$ to 1.87. The overall negative slope of the difference spectrum is due to that change in photon index. At the energy of the red wing of the Fe $K\alpha$ line there is a slight deficit with respect to the continuum. This implies that the red wing was stronger in the low flux state spectrum (as a result of the lower ξ) than in the high flux state spectrum. This feature is weak and very broad and is difficult to detect in the data. The difference spectrum

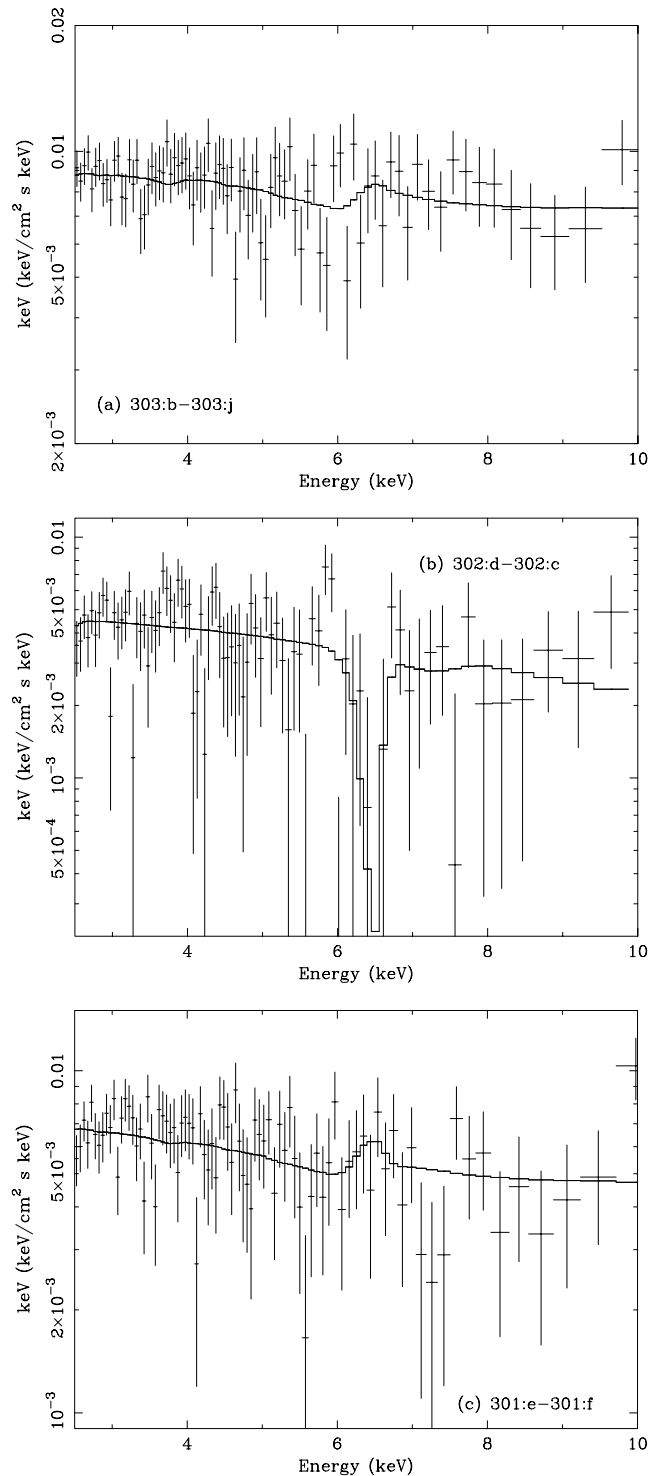


Figure 7. Unfolded spectra obtained from subtracting the best-fitting double-reflector model from a low flux state interval from the model of a high state segment. (a) The result when segment Rev. 303:j and 303:b (see Fig. 3) were used as the low and high flux states, respectively. These segments are separated by 70 ks. (b) The result when segment Rev. 302:c and 302:d were used as the low and high states. These intervals are adjacent to each other. (c) The result when segment Rev. 301:f and 301:e were used as the low and high states. These intervals are also adjacent to each other. See the text for the discussion of the interpretation.

also shows a hump at the position of the line core. This means that the 6.4-keV core was weaker in the low flux state than in the high flux state. If the distant reflector had equilibrated at the high flux state in segment 301:e, it would have not yet responded to the rapid decrease in flux unless the black hole mass was few $\times 10^6 M_{\odot}$; alternatively, it may be reacting to changes before the flare in 301:e, as it lasted only 10 ks (see Fig. 3).

The middle panel of Fig. 7 plots the difference between Rev. 302:d and 302:c, which illustrates the case of the source moving from a ‘steady’ low state (Rev. 302:a,b,c all have roughly the same flux) to a bright flare that occurs at the end of the Rev. 302:d. Fig. 3 shows that the pn count rate increased by nearly a factor of 2 over the 10-ks interval. The difference spectrum of these two segments shows a large (factor of 10) drop at ~ 6.5 keV, implying that the core of the Fe $K\alpha$ line was stronger in 302:c than in 302:d, opposite to what is expected if the line core was responding to the continuum on time-scales of ~ 10 ks.

The top panel of Fig. 7 shows the difference spectrum between two segments, which are separated by 70 ks. The ionization parameter for the data of Rev. 303:b is $\log \xi = 3.95$, while it is $\log \xi = 3.57$ for segment 303:j. Thus, the red wing of the Fe $K\alpha$ line, which originates from the ionized reflector should be stronger in the low flux state spectrum. This does seem to be the case, as the difference spectrum shows the profile of the red wing as a deficit between 3 and 6.4 keV, which means that this part of the spectrum is stronger in the low flux state spectrum than in the high flux state. The core of the line is marginally weaker in the low state than in the high flux state, consistent with the lower flux level. Yet, both of these features are < 10 per cent from the continuum, and again, as seen from the data points, difficult to detect unambiguously. The 2σ upper limit on the EW of any Gaussian feature at 6.5 keV in the data difference spectrum of 303:b and 303:j is 120 eV (it is 230 eV for 301:e and 301:f).

The conclusion from these tests is that this model does predict changes in the line profile on short time-scales, in particular around the red wing. However, these changes will be slight due to the breadth of the feature and that is why they have not been detected before. Unfortunately, higher signal-to-noise ratio data at small time-scales will be needed to check these predictions. Finally, the model also finds that small changes in the 6.4-keV line core are consistent with the data, but we are unable to determine a time-scale for the changes. Such variations have not been seen before (e.g. Reynolds 2000), and will need to be found for this multiple reflection model to be viable, although the signature may be complex. For example, a warped accretion disc is subject to Lense–Thirring precession, and this would cause variability in the outer reflector. Although a numerical simulation is needed to fully model the dynamics of such systems (Armitage & Natarajan 1999), the precession period can be estimated from (Bardeen & Petterson 1975)

$$t_{\text{prec}} \approx 5 \times 10^7 \left(\frac{a}{0.998} \right)^{-1} \left(\frac{M}{10^7 M_{\odot}} \right) \left(\frac{r}{70 r_g} \right)^3, \quad (1)$$

where a is the black hole spin parameter. Therefore, precession can only cause long time-scale variability in this model.

5.2.4 The inner annulus

Thus far we have ignored the problem that this model predicts that the primary X-ray emission originates from within a tiny annulus at $5r_g$. The fit converged to this value by fitting a notch in the spectrum at ~ 3.6 keV; in order for this to remain unblurred, the outer radius

was forced to be close to the inner radius, which is constrained by the width of the red wing. Replacing the pn data with the MOS data does not affect this result. It is possible that this feature is an emission line from hydrogenic argon from the outer reflector, which is not included in the reflection models. Further work needs to be performed to eliminate this possibility.

The requirement for the emission to be constrained to an annulus is very extreme as viscous dissipation throughout the accretion disc should go as r^{-3} (Shakura & Sunyaev 1973). If most of the accretion energy is transported to a magnetic corona above the disc then it could only be efficient in this small annulus, which seems highly unlikely given that magnetic fields will be present throughout the flow. In the 1997 flare spectrum reported by Iwasawa et al. (1999), they also found that the line emission seemed to arise from an annulus around $5r_g$. One explanation considered by these authors was that this emission was caused by a flare rotating along the very inner edge of the disc. However, as these authors pointed out, this implied a black hole mass greater than $10^8 M_{\odot}$ and theoretical problems concerning the height of the flare. In the model considered here, emission from an annulus at $5r_g$ is required at nearly every point in the observation, and cannot be due to a transient event such as a flare.

One possible explanation for this energy generation is a connection between a spinning black hole and the accretion disc (e.g. Blandford & Znajek 1977; Li 2000, 2002a,b). This was considered by Wilms et al. (2001) to explain the steep emissivity profile found in an earlier *XMM-Newton* observation of MCG–6-30-15. Since emission is required from within $6r_g$ it is likely that the black hole is spinning, and is therefore a source of energy that can be transformed into radiation. Returning radiation is another method to increase the emissivity of the inner disc (Martocchia, Matt & Karas 2002; Fabian & Vaughan 2002).

6 CONCLUSIONS

Making progress in the study of accretion discs and AGN can only be made by comparing models with data. Here, we have used the sophisticated ionized disc models of Ross & Fabian (1993) to fit the latest *XMM-Newton* and *BeppoSAX* spectrum of MCG–6-30-15. An ionized disc has often been considered as a possible explanation for the strange variability behaviour of the broad Fe $K\alpha$ line.

We found that an ionized disc model can fit the data and account for the spectral variability if there are two distinct reflection regions on the disc. This model requires a very specific geometry in order to be viable, but can be tested by searching for soft X-ray emission lines that are broadened to a few 10s of eV, but are not asymmetric, and, in the future, by the continuum variability properties above 30 keV. An apparent problem with this scenario is that it constrains ~ 80 per cent of the total X-ray flux of MCG–6-30-15 to be produced within a very narrow annulus only $5r_g$ from the black hole. This is a stringent requirement that is difficult to explain with standard AGN theory. Nevertheless, the advantage of the double-reflection model is that it can naturally explain the strange Fe $K\alpha$ line variability that has been previously observed. Time-resolved spectral fitting found that the inner reflector becomes more ionized as the source brightens, weakening the red wing of the iron line. Changes in the 6.4-keV line core are also found in the time-resolved fitting, but they do not necessarily correlate with the continuum. The model can also account for the $R > 2$ constraint implied by the *BeppoSAX* data by combining the reflection humps of multiple reprocessors.

One similarity that the model presented here has with previous work (Wilms et al. 2001; Fabian et al. 2002b) is the need for extra

production of radiation within $6r_g$. Therefore, irrespective of the number of reflectors or the ionization state of the disc, it seems likely there is some new physical process near the black hole of MCG-6-30-15 that needs to be untangled.

ACKNOWLEDGMENTS

Based on observations obtained with *XMM-Newton*, an ESA science mission with instruments and contributions directly funded by ESA Member States and the USA (NASA). DRB acknowledges financial support from the Commonwealth Scholarship and Fellowship Plan and the Natural Sciences and Engineering Research Council of Canada. ACF thanks the Royal Society for support. We thank the anonymous referee for useful comments.

REFERENCES

- Armitage P.J., Natarajan P., 1999, *ApJ*, 525, 909
 Arnaud K.A., 1996, in Jacoby G., Barnes J., eds, *ASP Conf. Ser. Vol. 101*, *Astronomical Data Analysis Software and Systems V*. Astron. Soc. Pac., San Francisco, p. 17
 Ballantyne D.R., Fabian A.C., 2001, *MNRAS*, 328, L11
 Ballantyne D.R., Ross R.R., 2002, *MNRAS*, 332, 777
 Ballantyne D.R., Iwasawa K., Fabian A.C., 2001a, *MNRAS*, 323, 506
 Ballantyne D.R., Ross R.R., Fabian A.C., 2001b, *MNRAS*, 327, 10
 Ballantyne D.R., Fabian A.C., Ross R.R., 2002, *MNRAS*, 329, L67
 Bardeen J.M., Petterson J.A., 1975, *ApJ*, 195, L65
 Beloborodov A.M., 1999, *ApJ*, 510, L123
 Blackman E.G., 1999, *MNRAS*, 306, L25
 Blandford R.D., Znajek R.L., 1977, *MNRAS*, 179, 433
 Branduardi-Raymont G., Sako M., Kahn S.M., Brinkman A.C., Kaastra J.S., Page M., 2001, *A&A*, 365, L140
 Chiang J., Reynolds C.S., Blaes O.M., Nowak M.A., Murray N., Madajski G., Marshall H.L., Magdziarz P., 2000, *ApJ*, 528, 292
 De Rosa A., Fabian A.C., Piro L., 2002a, *MNRAS*, 334, L21
 De Rosa A., Piro L., Fiore F., Grandi P., Maraschi L., Matt G., Nicastro F., Petrucci P.O., 2002b, *A&A*, 387, 838
 Dumont A.-M., Czerny B., Collin S., Życki P.T., 2002, *A&A*, 387, 63
 Elvis M., Wilkes B.J., Lockman F.J., 1989, *AJ*, 97, 777
 Fabian A.C., Vaughan S., 2003, *MNRAS*, in press (astro-ph/0301588)
 Fabian A.C., Rees M.J., Stella L., White N.E., 1989, *MNRAS*, 238, 729
 Fabian A.C., Ballantyne D.R., Merloni A., Vaughan S., Iwasawa K., Boller Th., 2002a, *MNRAS*, 331, L35
 Fabian A.C. et al., 2002b, *MNRAS*, 335, L1
 Fiore F., Guainazzi M., Grandi P., 1999, *Cookbook for BeppoSAX NFI Spectral Analysis*. Available from <http://www.asdc.asi.it/bepposax/software/index.html>
 Galeev A.A., Rosner R., Vaiana G.S., 1979, *ApJ*, 229, 318
 George I.M., Fabian A.C., 1991, *MNRAS*, 249, 352
 Guainazzi M. et al., 1999, *A&A*, 341, L27
 Haardt F., Maraschi L., 1991, *ApJ*, 380, L51
 Haardt F., Maraschi L., 1993, *ApJ*, 413, 507
 Ivanov P.B., Illarionov A.F., 1997, *MNRAS*, 285, 394
 Iwasawa K. et al., 1996, *MNRAS*, 282, 1038
 Iwasawa K., Fabian A.C., Young A.J., Inoue H., Matsumoto C., 1999, *MNRAS*, 306, L19
 Kumar S., Pringle J.E., 1985, *MNRAS*, 213, 435
 Laor A., 1991, *ApJ*, 376, 90
 Lee J.C., Fabian A.C., Brandt W.N., Reynolds C.S., Iwasawa K., 1999, *MNRAS*, 310, 973
 Lee J.C., Fabian A.C., Reynolds C.S., Brandt W.N., Iwasawa K., 2000, *MNRAS*, 318, 857
 Lee J.C., Ogle P.M., Canizares C.R., Marshall H.L., Schulz N.S., Morales R., Fabian A.C., Iwasawa K., 2001, *ApJ*, 554, L13
 Lee J.C., Iwasawa K., Houck J.C., Fabian A.C., Marshall H.L., Canizares C.R., 2002, *ApJ*, 570, L47
 Li L.-X., 2000, *ApJ*, 533, L115
 Li L.-X., 2002a, *ApJ*, 567, 463
 Li L.-X., 2002b, *A&A*, 392, 469
 Magdziarz P., Zdziarski A.A., 1995, *MNRAS*, 273, 837
 Malzac J., Beloborodov A.M., Poutanen J., 2001, *MNRAS*, 326, 417
 Martocchia A., Matt G., Karas V., 2002, *A&A*, 383, L23
 Matt G., Perola G.C., 1992, *MNRAS*, 259, 433
 Matt G., Perola G.C., Piro L., 1991, *A&A*, 247, 25
 Matt G., Fabian A.C., Ross R.R., 1993, *MNRAS*, 262, 179
 Matt G., Fabian A.C., Ross R.R., 1996, *MNRAS*, 278, 1111
 Misra R., 2001, *MNRAS*, 320, 445
 Nandra K., Pounds K.A., 1992, *Nat*, 359, 215
 Nandra K., Pounds K.A., 1994, *MNRAS*, 268, 405
 Nayakshin S., Kazanas D., Kallman T., 2000, *ApJ*, 537, 833
 Nelson R.P., Papaloizou J.C.B., 2000, *MNRAS*, 315, 570
 Orr A., Barr P., Guainazzi M., Parmar A.N., Young A.J., 2001, *A&A*, 376, 413
 Péquignot D. et al., 2001, in Ferland G.J., Savin D.W., eds, *ASP Conf. Ser. Vol. 247, Spectroscopic Challenges of Photoionized Plasmas*. Astron. Soc. Pac., San Francisco, p. 533
 Pounds K.A., Nandra K., Stewart G.C., George I.M., Fabian A.C., 1990, *Nat*, 344, 132
 Pringle J.E., 1996, *MNRAS*, 281, 357
 Pringle J.E., 1997, *MNRAS*, 292, 136
 Reynolds C.S., 2000, *ApJ*, 533, 811
 Reynolds C.S., Fabian A.C., 1997, *MNRAS*, 290, L1
 Reynolds C.S., Nowak M.A., 2003, *Phys. Rep.*, 377, 389
 Reynolds C.S., Fabian A.C., Nandra K., Inoue H., Kunieda H., Iwasawa K., 1995, *MNRAS*, 277, 901
 Ross R.R., Fabian A.C., 1993, *MNRAS*, 261, 74
 Ross R.R., Fabian A.C., Young A.J., 1999, *MNRAS*, 306, 461
 Ross R.R., Fabian A.C., Ballantyne D.R., 2002, *MNRAS*, 336, 315
 Różańska A., Dumont A.-M., Czerny B., Collin S., 2002, *MNRAS*, 332, 799
 Sako M. et al., 2002, *ApJ*, submitted (astro-ph/0112436)
 Shakura N.L., Sunyaev R.A., 1973, *A&A*, 24, 337
 Shih D.C., Iwasawa K., Fabian A.C., 2002, *MNRAS*, 333, 687
 Stella L., 1990, *Nat*, 344, 747
 Strüder L. et al., 2001, *A&A*, 365, L18
 Tanaka Y. et al., 1995, *Nat*, 375, 659
 Vaughan S., Edelson R., 2001, *ApJ*, 548, 694
 White T.R., Lightman A.P., Zdziarski A.A., 1988, *ApJ*, 331, 939
 Wilms J., Reynolds C.S., Begelman M.C., Reeves J., Molendi S., Staubert R., Kendziorra E., 2001, *MNRAS*, 328, L27

This paper has been typeset from a $\text{\TeX}/\text{\LaTeX}$ file prepared by the author.